




Article

Phase Transitions and Electric Properties of PbBr_2 under High Pressure: A First-Principles Study

Lihua Yang^{1,2} , Yukai Zhang¹, Yanli Chen¹ , Xin Zhong¹, Dandan Wang¹, Lin Fan¹, Jihui Lang¹, Xin Qu^{1,*}  and Jinghai Yang^{1,*}

¹ Key Laboratory of Functional Materials Physics and Chemistry of the Ministry of Education, College of Physics, Jilin Normal University, Siping 136000, China

² State Key Laboratory of Integrated Optoelectronics, College of Materials Science and Engineering, Jilin University, Changchun 130012, China

* Correspondence: quxin515@163.com (X.Q.); jhyang1@jlnu.edu.cn (J.Y.)

Abstract: PbBr_2 has recently attracted considerable attention as a precursor for lead halide perovskite-based devices because of its attractive properties. It is known that pressure can modify the chemical and physical properties of materials by altering the distance between atoms in the lattice. Here, a global structure-searching scheme was used to explore the high-pressure structures of PbBr_2 , whose structures and properties at high pressure are still far from clear. Three new phases of PbBr_2 were predicted in the pressure range of 0–200 GPa, and the pressure-driven phase transition sequence of orthorhombic Pnma (0–52 GPa) \rightarrow tetragonal I4/mmm (52–80 GPa) \rightarrow orthorhombic Cmca (80–153.5 GPa) \rightarrow orthorhombic Immm (153.5–200 GPa) is proposed. Electronic calculations indicate a semiconductor-to-metallic transition of PbBr_2 in the Cmca phase at \sim 120 GPa. Our present results could be helpful in improving the understanding of fundamental physical properties and provide insights to modulate the structural and related photoelectric properties of PbBr_2 .

Keywords: high pressure; structure prediction; simulation; structural evolution; lead halide



Citation: Yang, L.; Zhang, Y.; Chen, Y.; Zhong, X.; Wang, D.; Fan, L.; Lang, J.; Qu, X.; Yang, J. Phase Transitions and Electric Properties of PbBr_2 under High Pressure: A First-Principles Study. *Materials* **2022**, *15*, 8222. <https://doi.org/10.3390/ma15228222>

Academic Editor: Bryan M. Wong

Received: 17 October 2022

Accepted: 15 November 2022

Published: 19 November 2022

Publisher's Note: MDPI stays neutral with regard to jurisdictional claims in published maps and institutional affiliations.



Copyright: © 2022 by the authors. Licensee MDPI, Basel, Switzerland. This article is an open access article distributed under the terms and conditions of the Creative Commons Attribution (CC BY) license (<https://creativecommons.org/licenses/by/4.0/>).

1. Introduction

Lead bromide (PbBr_2) is drawing attention due to significant scientific and technological applications. The presence of Pb with a high effective atomic number ($Z_{\text{eff}} = 82$) enables PbBr_2 to have a superior absorption ability for high-energy photons, so that PbBr_2 could be applied in X-ray or γ -ray detection [1–3]. Due to its good acousto-optic merit and wide transmission range, PbBr_2 has been applied in acousto-optic devices [4–7]. The crystal growth, purification, and optical and acoustic character of PbBr_2 have been studied over the past few decades [6–10]. Recently, PbBr_2 has been used extensively to prepare perovskite-based devices, such as the hybrid perovskites solar cells [11–13], photodetectors [14], led light-based devices [15], photocatalysts of antibiotics [16] and luminescent complexes in solvents [17,18].

It is known that pressure can alter the chemical and physical properties of materials as it can adjust the distance between atoms in the lattice [19–24]. At ambient conditions, PbBr_2 is a semiconductor material and crystallizes in a cotunnite phase (Pnma, $Z = 4$) similar to many other AB_2 compounds [9,10,25,26]. Theoretical and experimental studies on the electronic properties and structural transition sequences under high pressure for PbBr_2 are less investigated, hindering the in-depth exploration of the chemical and physical properties of PbBr_2 under compression. Thus, it is essential to investigate the structural evolution of PbBr_2 under pressure for the further design of lead halide perovskite photovoltaics.

In this work, we explored the structures of PbBr_2 by the well-known CALYPSO structure searches method, combined with first-principles calculations at a wide pressure range of 0–200 GPa. Our results show that the pressure-driven structural evolution of PbBr_2 is orthorhombic Pnma \rightarrow tetragonal I4/mmm \rightarrow orthorhombic Cmca \rightarrow orthorhombic

Immm phase with transition pressures of 52, 80 and 153.5 GPa, respectively. We further investigated the PbBr_2 electronic properties under high pressure. Strikingly, the phase transition is accompanied by a semiconductor-to-metallic transition. Our results will advance the understanding of the structure and electronic properties of PbBr_2 under extreme conditions.

2. Materials and Methods

Structure searches for PbBr_2 were carried out by the CALYPSO method (by registering at <http://www.calypso.cn>, accessed on 5 June 2013) [27–29], which was verified successfully by many studies [30–37]. Each generation contained 50 structures, and the first generation was produced randomly with symmetry constraints. All structures were locally optimized using the VASP code [38]. Local optimizations performed during structure search were undertaken with the conjugate gradients method and were stopped when enthalpy changes became smaller than 1×10^{-5} eV per cell. Sixty percent of the lowest-enthalpy structures of each generation were used to produce the structures in the next generation by local Particle Swarm Optimization techniques, and the remaining 40% of structures were randomly generated within symmetry constraints to enhance structural diversity. During the structure searches, each newly generated structure was subjected to structural optimization at target pressures to obtain local-minimum configurations. All structure optimization, enthalpy and electronic properties calculations adopt the VASP code with the generalized gradient approximation functional (Perdew–Burke–Ernzerh) [39]. We employ the projector augmented wave [40] scheme to treat the valence electrons of Pb and Br as $5d^{10} 6s^2 6p^2$ and $3d^{10} 4s^2 4p^5$. A total of 1000–1200 structures were generated for each structure search calculation with an energy cutoff of 310 eV. To ensure convergence of the calculated data, a kinetic energy cutoff of 400 eV and dense k-point sampling with a grid spacing of 0.2 \AA^{-1} were employed. We used the PHONOPY code to ensure dynamical stabilities of the predicted PbBr_2 structures [25]. Electron localization functions (ELFs) were drawn using VESTA software [41].

3. Results and Discussion

To discover stable structures of PbBr_2 at high pressure, we executed systematic structural searches with 1–4 formula units at 0, 20, 50, 100, 150 and 200 GPa. According to our simulations, four energetically stable PbBr_2 phases were found and are shown in Figure 1a–d. At 0 and 20 GPa, we reproduced the experimental Pnma structure (4 f.u., $Z = 4$). The unit-cell parameters of the predicted Pnma structure are very close to the experiment data [6,10], demonstrating the validity of the simulated method adopted here. As shown in Figure 1a, the Pb atom is ninefold coordinated by Br. Both Pb and Br atoms are located on the fourfold 4c site. Above 52 GPa, the already known PbBr_2 with Pnma symmetry transforms into a tetragonal structure with $I4/mmm$ ($Z = 2$) symmetry, accompanied by the nearest Br–Br distances shortened from 3.26 Å (at 20 GPa) to 2.88 Å (at 60 GPa). In the $I4/mmm$ structure, Pb and Br atoms occupy the 2b site and 4e site, respectively. Within this structure, each Pb atom is tenfold coordinated by Br, forming a PbBr_{10} square prism with a double cap. At 60 GPa, the distance from the central Pb atom to the side Br1 atom and capped Br2 atoms of the prism is 2.836 Å and 3.022 Å, respectively. The Pnma and $I4/mmm$ structures of PbBr_2 are also predicted to exist in PbI_2 and BaI_2 [42,43].

Upon increasing the pressure to 80 GPa, PbBr_2 adopts an orthorhombic Cmca structure with $Z = 8$. This structure can be seen as symmetry lowering of the $I4/mmm$ structure. Within the Cmca structure (Figure 1c), Pb and Br atoms occupy the Wyckoff 8f site and 16g site, respectively, and the nearest Br–Br is 2.73 Å at 100 GPa. At a pressure above 153.5 GPa, an orthorhombic Immm ($Z = 8$) phase was found to be most stable up to 200 GPa. Significantly, the current PbBr_2 Immm structure differs from the Immm structure found in PbI_2 (Immm-I) [42]. While the former structure (Figure 1d) contains two distinct Pb atoms occupying the 4i and 4h sites, and four Br atoms occupying 2b, 2d, 4g, and 8l, respectively, the later has 2 f.u. in a unit cell with the Pb and I atoms occupying the Wyckoff 2d site and

4f site (the enthalpy difference of two Immm phases was calculated in Figure 2a). Within the Immm structure of PbBr_2 , the Pb atoms are tenfold coordinated, and the nearest Br–Br is 2.57 Å at 200 GPa. In conclusion, the Br–Br distances in the four stable PbBr_2 structures are much smaller than those in pure Br_2 (2.27 Å), indicating that no Br–Br covalent bond is formed.

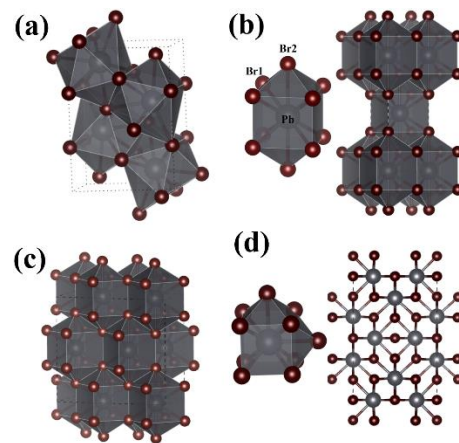


Figure 1. Crystal structures of stable PbBr_2 : (a) Pnma at 20 GPa, (b) I4/mmm at 60 GPa, (c) Cmca at 100 GPa, and (d) Immm at 200 GPa.

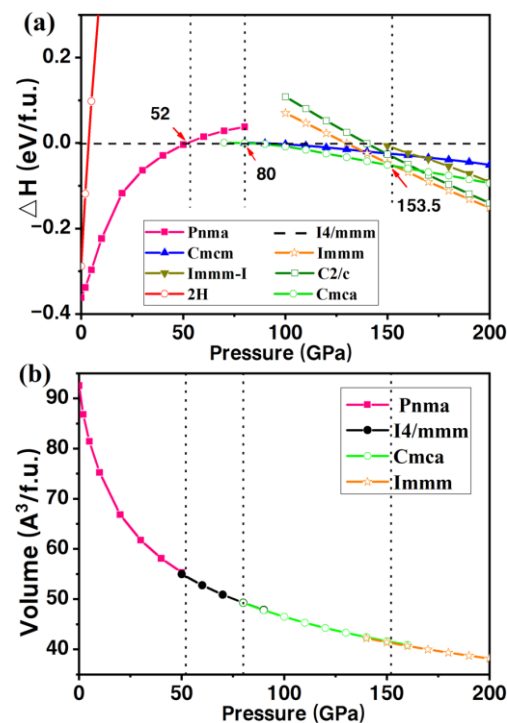


Figure 2. (a) Enthalpies related to the I4/mmm phase. (b) Relative volume of four stable PbBr_2 phases.

We calculated the enthalpy difference (ΔH) of four stable PbBr_2 phases relative to I4/mmm PbBr_2 , as shown in Figure 2a. Several structures in a previous study on lead halide compounds [42] were also considered. Obviously, the four PbBr_2 structures we searched have the lower enthalpies. The changes in volume as a function of pressure of the predicted PbBr_2 are also plotted in Figure 2b. The continuous change of unit cell volume of PbBr_2 with pressure suggests a second-order structural phase transition. Our work suggests that PbBr_2 follows the structural transition order of Pnma (0–52 GPa) \rightarrow I4/mmm (52–80 GPa) \rightarrow Cmca (80–153.5 GPa) \rightarrow Immm (153.5–200 GPa). Our phonon

calculations demonstrate the dynamic stability of all these predicted PbBr_2 structures, as shown in Figure 3. The detailed structural parameters and calculated phonon spectra of the predicted PbBr_2 phases are shown in Table 1.

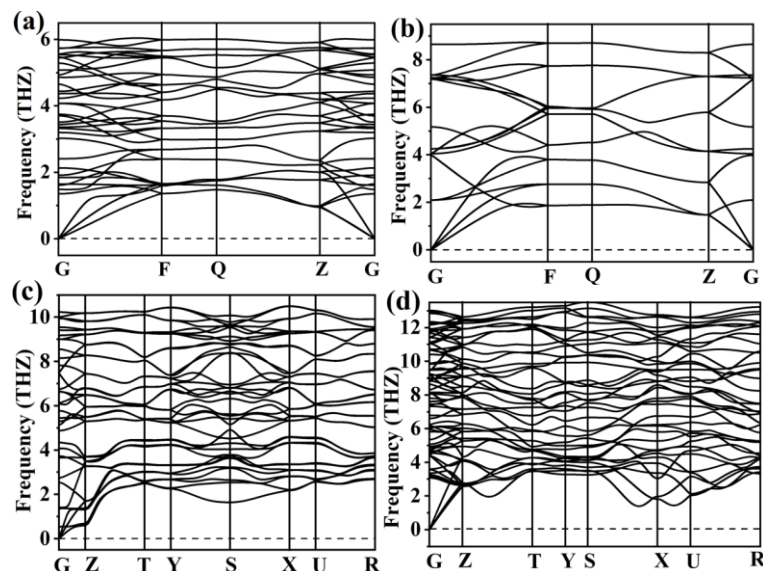


Figure 3. Phonon dispersion curves of stable PbBr_2 : (a) Pnma at 20 GPa, (b) I4/mmm at 60 GPa, (c) Cmca at 100 GPa, and (d) Immm at 200 GPa.

Table 1. Lattice parameters and atomic coordinates of a conventional unit cell of PbBr_2 .

Phase	Z	Lattice (Å)	Atom	X	Y	Z
Pnma 0 GPa	4	a = 8.04246	Pb(4c)	0.734	0.750	0.910
		b = 4.76121	Br1(4c)	0.516	0.750	0.162
		c = 9.66722	Br2(4c)	0.358	0.250	0.418
I4/mmm 60 GPa	2	a = b = 3.426	Pb(2a)	0.000	0.000	0.000
		c = 8.993	Br(4e)	0.000	0.000	0.336
Cmca 100 GPa	8	a = 8.548	Pb(8f)	0.000	0.790	0.875
		b = 4.679	Br(16g)	−0.166	0.295	0.875
		c = 9.295				
$\alpha = \beta = \gamma = 90$						
Immm 200 GPa	8	a = 3.598	Pb1(4i)	0.000	0.000	0.241
		b = 11.177	Pb2(4h)	0.000	0.824	0.500
		c = 7.594	Br1(2d)	0.500	0.000	0.500
		$\alpha = \beta = \gamma = 90$	Br2(4g)	0.000	0.837	0.000
			Br3(8l)	0.500	0.833	0.253
Br4(2b)	0.500	0.000	0.000			

In order to further research the bonding properties of PbBr_2 under compression, we investigated the ELF of four stable PbBr_2 phases. All phases share similar features. We present the ELF of the I4/mmm phase in Figure 4 as a representative. The blue color corresponding to the ELF value < 0.5 is mostly around Pb atoms, indicating the electron shortage of Pb and electron transfer from Pb to Br. Because the ELF map does not show electron localization at the lattice gap, the bonding type between Pb and Br is mainly ionic. The isosurface of ELF with a value of 0.7 (Figure 4b) also indicates an electronic consumption near Pb atoms and cumulation around Br atoms, showing the charge transfer from Pb to Br, associated with the Pb–Br ionic bond.

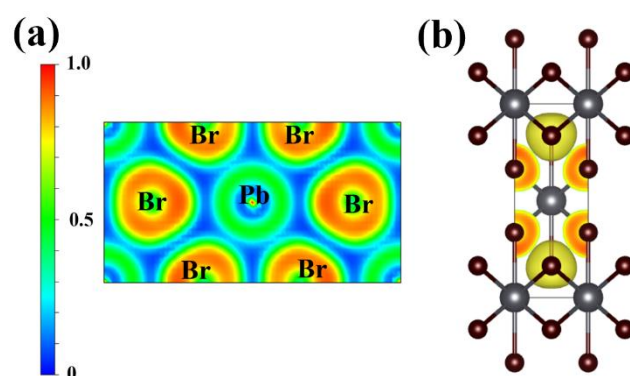


Figure 4. (a) 2D ELF plot through the (1-10) plane and (b) isosurface of the ELF plot with a value of 0.7 for $I4/mmm$ $PbBr_2$ at 60 GPa. Big spheres represent Pb atoms; small spheres denote Br atoms.

We calculated the electronic band and partial density of states (PDOS) of the four predicted structures. The $Pnma$ phase is a semiconductor with an indirect bandgap $E_g = 2.11$ eV, where the Pb-6p and Br-5p states dominate the valence band (VB) edge, and an anti-bonding hybridization of the Pb-6s and Br-5p states controls the conduction band (CB) edge, as shown in Figure 5a. The bonding character of the $I4/mmm$ phase is similar to that in the $Pnma$ structure, e.g., the band structure calculated at 60 GPa also shows an indirect band gap ($E_g = 0.69$ eV). The $I4/mmm$ structure remains a semiconductor at the pressure stability interval (52–80 GPa). For the $Cmca$ structure of $PbBr_2$, the calculated band structures at 80, 120 and 140 GPa show that a semiconductor–metal transition occurs at ~ 120 GPa, because the CB extends across the Fermi level (Figure 5c–e). It can be seen that lead bromide metallizes at a higher pressure than lead iodide (~ 27 GPa). In the high-pressure $Immm$ phase of $PbBr_2$, both the VB and CB extend across the Fermi level, and the metallic nature of $PbBr_2$ persists up to 200 GPa.

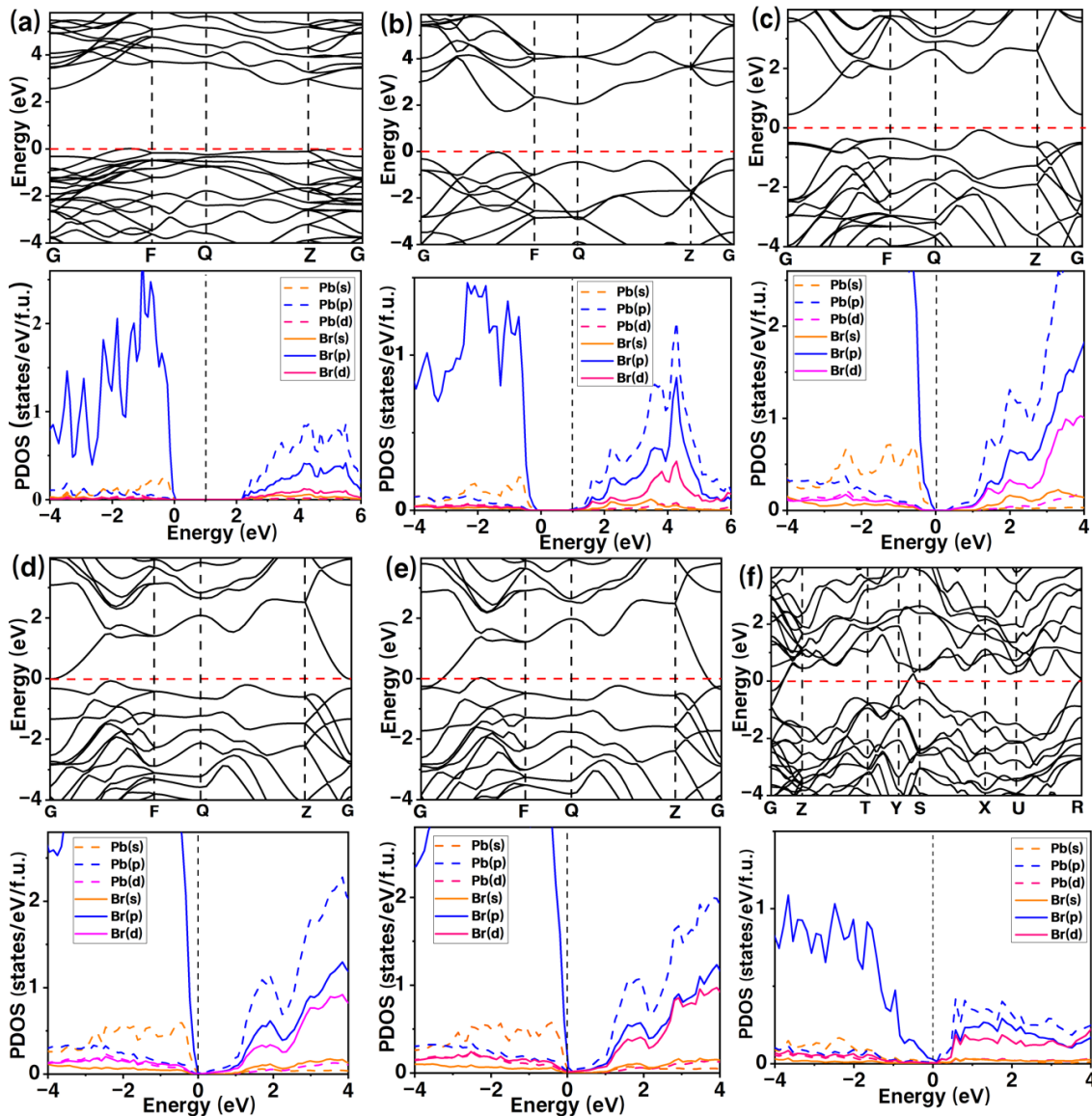


Figure 5. Calculated electronic band (**top**) and PDOS (**bottom**) plot of predicted PbBr_2 phases: (a) Pnma at 20 GPa, (b) $I4/mmm$ at 60 GPa, (c–e) Cmca at 80, 120, 140 GPa, and (f) Immm at 200 GPa, respectively.

4. Conclusions

We studied the pressure-driven structural transformation and electronic properties of PbBr_2 up to 200 GPa. The structural evolution of PbBr_2 is orthorhombic Pnma \rightarrow tetragonal $I4/mmm$ \rightarrow orthorhombic Cmca \rightarrow orthorhombic Immm phase with transition pressures of 52, 80 and 153.5 GPa, respectively. Electronic calculations indicate that Pnma and $I4/mmm$ phases are semiconductors, and a semiconductor-to-metallic transition of PbBr_2 was found in the Cmca phase at ~ 120 GPa. The Immm phase maintains metallic properties throughout the pressure stabilization range. Our results will stimulate further studies on the behavior of AB_2 -type halides under extreme conditions.

Author Contributions: Investigation, Y.Z. and L.F.; data curation, D.W. and X.Z.; writing—original draft preparation, L.Y.; writing—review and editing, X.Q. and Y.C.; supervision, L.Y. and J.Y.; funding acquisition, J.L. All authors have read and agreed to the published version of the manuscript.

Funding: This research was funded by the National Natural Science Foundation of China, grant number 11904129, 22078124 and 61904066; the Program for the Development of Science and Technology of Jilin Province, grant numbers YDZJ202101ZYTS065 and 202002015JC; and the Research Project of the “13th Five-Year Plan” of Jilin Provincial Education Department, grant numbers JJKH20220423KJ.

Institutional Review Board Statement: Not applicable.

Informed Consent Statement: Not applicable.

Data Availability Statement: The data presented in this study are available on request from the corresponding authors.

Conflicts of Interest: The authors declare no conflict of interest.

References

1. Yanagida, T.; Fujimoto, Y.; Yoshikawa, A.; Yokota, Y.; Kamada, K.; Pejchal, J.; Chani, V.; Kawaguchi, N.; Fukuda, K.; Uchiyama, K.; et al. Development and Performance Test of Picosecond Pulse X-ray Excited Streak Camera System for Scintillator Characterization. *Appl. Phys. Express* **2010**, *3*, 056202. [[CrossRef](#)]
2. Torres, O.G.; Gordillo, G.; Plazas, M.C.; Téllez, D.A.L.; Roa-Rojas, J. Optical features of PbBr₂ semiconductor thin films for radiation attenuation application. *J. Mater. Sci. Mater. Electron.* **2021**, *32*, 16937–16944. [[CrossRef](#)]
3. Nikl, M. Scintillation detectors for X-rays. *Meas. Sci. Technol.* **2006**, *17*, R37–R54. [[CrossRef](#)]
4. Tubbs, M.R. The optical properties and chemical decomposition of halides with layer structures. I. crystal structures, optical properties, and electronic structure. *Phys. Status Solidi* **1972**, *49*, 11–50. [[CrossRef](#)]
5. Kusumoto, H.; Kaito, T.; Yanagiya, S.-I.; Mori, A.; Inoue, T. Growth of single crystals of PbBr₂ in silica gel. *J. Cryst. Growth* **2005**, *277*, 536–540. [[CrossRef](#)]
6. Kaito, T.; Yanagiya, S.-I.; Mori, A.; Kurumada, M.; Kaito, C.; Inoue, T. Characteristic nanocrystallite growth of PbBr₂ in a magnetic field in gel. *J. Cryst. Growth* **2006**, *294*, 407–410. [[CrossRef](#)]
7. Kaito, T.; Inoue, T.; Yanagiya, S.; Mori, A.; Masaki, K. Melt growth and characterization of PbBr₂ single crystals. *J. Cryst. Growth* **2005**, *275*, e721–e726. [[CrossRef](#)]
8. Ahmad, Z.; Mishra, A. Growth of PbBr₂ microrods with unique structure and surface morphology. *J. Mater. Sci. Mater. Electron.* **2020**, *31*, 4672. [[CrossRef](#)]
9. Girgis, S.Y.; Mady, K.A. Electrical conductivity of vacuum-deposited lead bromide layers. *J. Mater. Sci. Lett.* **1986**, *5*, 1091–1094. [[CrossRef](#)]
10. Varshney, S.; Chi, L.; Singh, C.V.; Nogami, J. Atomic structure of PbBr₂ thin films on Ag (111). *Solid State Commun.* **2022**, *343*, 114651. [[CrossRef](#)]
11. Mutalikdesai, A.; Ramasesha, S.K. Emerging solar technologies: Perovskite solar cell. *Resonance* **2017**, *22*, 1061–1083. [[CrossRef](#)]
12. Cleveland, I.J.; Tran, M.N.; Dey, A.; Aydil, E.S. Vapor deposition of CsPbBr₃ thin films by evaporation of CsBr and PbBr₂. *J. Vac. Sci. Technol. A* **2021**, *39*, 043415. [[CrossRef](#)]
13. Ren, Q.; Ding, L.-Y.; Chen, F.-S.; Cheng, R.-P.; Xu, D. The optical properties of lead bromide crystals. *J. Mater. Sci. Lett.* **1997**, *16*, 1247–1248. [[CrossRef](#)]
14. Liu, Y.; Zhang, Y.; Yang, Z.; Feng, J.; Xu, Z.; Li, Q.; Hu, M.; Ye, H.; Zhang, X.; Liu, M.; et al. Low-temperature-gradient crystallization for multi-inch high-quality perovskite single crystals for record performance photodetectors. *Mater. Today* **2019**, *22*, 67–75. [[CrossRef](#)]
15. Lan, J.; Luo, L.; Wang, M.; Li, F.; Wu, X.; Wang, F. One pot gram-scale synthesis of CsPbBr₃ nanocrystals and their application in green LED. *J. Lumin.* **2019**, *210*, 464–471. [[CrossRef](#)]
16. Zhao, Y.; Wang, Y.; Liang, X.; Shi, H.; Wang, C.; Fan, J.; Hu, X.; Liu, E. Enhanced photocatalytic activity of Ag-CsPbBr₃/CN composite for broad spectrum photocatalytic degradation of cephalosporin antibiotics 7-ACA. *Appl. Catal. B Environ.* **2019**, *247*, 57–69. [[CrossRef](#)]
17. Chin, S.-H.; Choi, J.W.; Hu, Z.; Mardegan, L.; Sessolo, M.; Bolink, H.J. Tunable luminescent lead bromide complexes. *J. Mater. Chem. C* **2020**, *8*, 15996–16000. [[CrossRef](#)]
18. Yin, J.; Zhang, Y.; Bruno, A.; Soci, C.; Bakr, O.M.; Brédas, J.-L.; Mohammed, O.F. Intrinsic Lead Ion Emissions in Zero-Dimensional Cs₄PbBr₆ Nanocrystals. *ACS Energy Lett.* **2017**, *2*, 2805–2811. [[CrossRef](#)]
19. Liu, Y.; Wang, R.; Wang, Z.; Li, D.; Cui, T. Formation of twelve-fold iodine coordination at high pressure. *Nat. Commun.* **2022**, *13*, 412. [[CrossRef](#)] [[PubMed](#)]
20. Zhang, L.; Wang, Y.; Lv, J.; Ma, Y. Materials discovery at high pressures. *Nat. Rev. Mater.* **2017**, *2*, 17005. [[CrossRef](#)]
21. Liu, R.; Xu, D.; Yao, Z.; Niu, S.; Liu, B. The New High-Pressure Phases of Nitrogen-Rich Ag–N Compounds. *Materials* **2022**, *15*, 4986. [[CrossRef](#)] [[PubMed](#)]
22. Li, S.; Wang, H.; Sun, W.; Lu, C.; Peng, F. Superconductivity in compressed ternary alkaline boron hydrides. *Phys. Rev. B* **2022**, *105*, 224107. [[CrossRef](#)]
23. Yang, L.; Qu, X.; Zhong, X.; Wang, D.; Chen, Y.; Lang, J.; Liu, C.; Sun, B.; Yang, J. The unconventionally stoichiometric compounds in the Na–K system at high pressures. *Comput. Mater. Sci.* **2021**, *200*, 110818. [[CrossRef](#)]

24. Qu, X.; Yang, L.; Lv, J.; Xie, Y.; Yang, J.; Zhang, Y.; Wang, Y.; Zhao, J.; Chen, Z.; Ma, Y. Particle Swarm Predictions of a SrB₈ Monolayer with 12-Fold Metal Coordination. *J. Am. Chem. Soc.* **2022**, *144*, 11120–11128. [[CrossRef](#)]
25. Togo, A.; Oba, F.; Tanaka, I. First-principles calculations of the ferroelastic transition between rutile-type and CaCl₂-type SiO₂ at high pressures. *Phys. Rev. B Condens. Matter Mater. Phys.* **2008**, *78*, 134106. [[CrossRef](#)]
26. Raman, A.; Steinfink, H. Crystal chemistry of AB₂ structures. *Inorg. Chem.* **1967**, *6*, 1789–1791. [[CrossRef](#)]
27. Wang, Y.; Lv, J.; Ma, Y.; Cui, T.; Zou, G. Superconductivity of MgB₂ under Ultra high Pressure: A First-Principles Study. *Phys. Rev. B* **2009**, *80*, 092505. [[CrossRef](#)]
28. Wang, Y.; Lv, J.; Zhu, L.; Ma, Y. CALYPSO: A Method for Crystal Structure Prediction. *Comput. Phys. Commun.* **2012**, *183*, 2063–2070. [[CrossRef](#)]
29. Lv, J.; Wang, Y.; Zhu, L.; Ma, Y. Particle-swarm structure prediction on clusters. *J. Chem. Phys.* **2012**, *137*, 084104. [[CrossRef](#)]
30. Lu, W.; Liu, S.; Liu, G.; Hao, K.; Zhou, M.; Gao, P.; Wang, H.; Lv, J.; Gou, H.; Yang, G.; et al. Disproportionation of SO₂ at High Pressure and Temperature. *Phys. Rev. Lett.* **2022**, *128*, 106001. [[CrossRef](#)]
31. Zhong, X.; Sun, Y.; Iitaka, T.; Xu, M.; Liu, H.; Hemley, R.J.; Chen, C.; Ma, Y. Prediction of Above-Room-Temperature Superconductivity in Lanthanide/Actinide Extreme Superhydrides. *J. Am. Chem. Soc.* **2022**, *144*, 13394–13400. [[CrossRef](#)]
32. Zhu, L.; Liu, H.; Pickard, C.J.; Zou, G.; Ma, Y. Reactions of Xenon with Iron and Nickel Are Predicted in the Earth's Inner Core. *Nat. Chem.* **2014**, *6*, 644–648. [[CrossRef](#)]
33. Li, Y.; Hao, J.; Liu, H.; Li, Y.; Ma, Y. The Metallization and Superconductivity of Dense Hydrogen Sulfide. *J. Chem. Phys.* **2014**, *140*, 174712. [[CrossRef](#)]
34. Li, Y.; Wang, L.; Liu, H.; Zhang, Y.; Hao, J.; Pickard, C.J.; Nelson, J.R.; Needs, R.J.; Li, W.; Huang, Y.; et al. Dissociation Products and Structures of Solid H₂S at Strong Compression. *Phys. Rev. B* **2016**, *93*, 020103. [[CrossRef](#)]
35. Li, X.; Zhang, X.; Bergara, A.; Gao, G.; Liu, Y.; Yang, G. Superconducting LaP₂H₂ with graphenelike phosphorus layers. *Phys. Rev. B* **2022**, *105*, 024504. [[CrossRef](#)]
36. Yan, X.; Ding, S.; Zhang, X.; Bergara, A.; Liu, Y.; Wang, Y.; Zhou, X.-F.; Yang, G. Enhanced superconductivity in CuH₂ monolayers. *Phys. Rev. B* **2022**, *106*, 014514. [[CrossRef](#)]
37. Lv, J.; Wang, Y.; Zhu, L.; Ma, Y. Predicted Novel High-Pressure Phases of Lithium. *Phys. Rev. Lett.* **2011**, *106*, 015503. [[CrossRef](#)]
38. Kresse, G.; Furthmüller, J. Efficient iterative schemes for ab initio total-energy calculations using a plane-wave basis set. *Phys. Rev. B* **1996**, *54*, 11169. [[CrossRef](#)]
39. Perdew, J.P.; Burke, K.; Ernzerhof, M. Generalized gradient approximation made simple. *Phys. Rev. Lett.* **1996**, *77*, 3865. [[CrossRef](#)]
40. Blochl, P.E. Projector Augmented-Wave Method. *Phys. Rev. B* **1994**, *50*, 17953. [[CrossRef](#)]
41. Momma, K.; Izumi, F. VESTA 3 for three-dimensional visualization of crystal, volumetric and morphology data. *J. Appl. Crystallogr.* **2011**, *44*, 1272–1276. [[CrossRef](#)]
42. Yang, L.; Zhang, Y.; Wang, J.; Wang, Y.; Yu, W.W. Pressure-induced phase transitions of lead iodide. *RSC Adv.* **2016**, *6*, 84604–84609. [[CrossRef](#)]
43. Wei, S.; Liu, H. High-Pressure Structures and Superconductivity of Barium Iodide. *Materials* **2022**, *15*, 522. [[CrossRef](#)]